Journal of Alloys and Compounds 639 (2015) 547–555

Contents lists available at ScienceDirect

Journal of Alloys and Compounds

journal homepage: www.elsevier.com/locate/jalcom

Mössbauer spectroscopy study of a new layered iron oxyselenide $Na_2Fe_2Se_2O$

Farshad Nejadsattari [a], Zbigniew M. Stadnik [a,*], Jan Żukrowski [b]

[a] Department of Physics, University of Ottawa, Ottawa, Ontario K1N 6N5, Canada
[b] Academic Centre for Materials and Nanotechnology, AGH University of Science and Technology, 30-059 Kraków, Poland

ARTICLE INFO

Article history:
Received 9 March 2015
Received in revised form 26 March 2015
Accepted 27 March 2015
Available online 1 April 2015

Keywords:
Blocked checkerboard antiferromagnetism
Mott insulator
Mössbauer spectroscopy

ABSTRACT

We report the results of ^{57}Fe Mössbauer spectroscopy study, complemented by first-principles energy-band structure and the hyperfine-interaction parameters calculations, of a recently discovered layered iron oxyselenide $Na_2Fe_2Se_2O$. It is confirmed that $Na_2Fe_2Se_2O$ is a Mott insulator. It is demonstrated experimentally that $Na_2Fe_2Se_2O$ orders antiferromagnetically with the Néel temperature $T_N = 74.8(2)$ K and with the Fe magnetic moment of $3.0(1)\,\mu_B$. The calculated hyperfine-interaction parameters are in good agreement with the corresponding experimental parameters. The Debye temperature of $Na_2Fe_2Se_2O$ is found to be 274(3) K.

1. Introduction

The recent discovery of high-T_C superconductivity in iron-based compounds [1–4] has led to a renewed interest in studies of complex oxides with layered structures [5]. This interest has been precipitated by the observation that the crystal structure of the Fe-based superconductors is very similar, or the same, as that of some complex oxide compounds.

Layered *d*-metal pnictide oxides $Na_2Ti_2Pn_2O$, with pnictide *Pn* = Sb and As, that were synthesized for the first time by Adam and Schuster [6], have a layered structure (a tetragonal unit cell with $I4/mmm$ space group) resembling the structure of cuprate high-T_C superconductors such as $La_{2-x}Ba_xCuO_{4-\delta}$ [7]. This structure consists of an alternation of the $Ti_2Pn_2O^{2-}$ layer and the Na^+ double layer [6,8,9]. The anomalous temperature dependences of the electrical resistivity, magnetic susceptibility [8–11], and other physical quantities [12] in $Na_2Ti_2Pn_2O$ were taken as evidence for the occurrence of a charge- or spin-density wave instability [13,14]. These anomalous temperature dependences suggest the possibility of antiferromagnetic order in the $Na_2Ti_2Pn_2O$ compounds, but no such order has been yet detected [10]. Theoretical calculations by Picket [13] show that Ti ions in $Na_2Ti_2Pn_2O$ show no inclination to carry a magnetic moment, whereas the recent calculations by Yan and Lu [15] predict that $Na_2Ti_2As_2O$ is a novel blocked checkerboard antiferromagnetic semiconductor and that $Na_2Ti_2Sb_2O$ is a bi-collinear antiferromagnetic semimetal. The experimentally observed anomalous dependences of various physical quantities in the $Na_2Ti_2Pn_2O$ compounds [8–12] are quite similar to those observed in some oxypnictide parent compounds of high-T_C iron-based superconductors. One could thus even consider pnictide oxides $Na_2Ti_2Pn_2O$ as possible superconductor parent compounds.

Very recently, a new layered oxyselenide $Na_2Fe_2Se_2O$ was successfully synthesized [16]. It has the same structure as that of $Na_2Ti_2Pn_2O$, that is, it is built by alternately stacking along the *c* axis the edge-shared $[Fe_2Se_2O]^{2-}$ layers and the double layers of Na^+ [16]. The recent *ab-initio* study of $Na_2Fe_2Se_2O$ predicts [17] that this compound is a Mott insulator with the Fe magnetic moments antiferromagnetically coupled in a blocked checkerboard configuration. In the present work, we have used ^{57}Fe Mössbauer spectroscopy to determine experimentally the type of magnetic ordering and several hyperfine-interaction properties in this new oxyselenide. In addition, *ab-initio* calculations of the energy band structure and of the hyperfine-interaction parameters of this compound have been carried out.

2. Theoretical and experimental methods

Polycrystalline samples of nominal composition $Na_2Fe_2Se_2O$ were synthesized by solid-state reaction, as described earlier [16]. The compound studied crystallizes in the anti-K_2NiF_4 structure type [space group $I4/mmm$ (No. 139)] with the room-temperature lattice constants $a = 4.107(8)$ Å and $c = 14.641(8)$ Å [16]. The studied $Na_2Fe_2Se_2O$ is a single-phase compound because no impurities could be detected in its X-ray diffraction spectrum [16].

Ab initio calculations of several physical properties of $Na_2Fe_2Se_2O$ have been performed within the framework of density functional theory using the full-potential linearized augmented-plane-wave plus local orbitals (FP-LAPW+lo) method as implemented in the WIEN2k package [18]. In this method, the unit cell is

* Corresponding author.
E-mail address: stadnik@uottawa.ca (Z.M. Stadnik).

http://dx.doi.org/10.1016/j.jallcom.2015.03.200
0925-8388/

partitioned into two regions: a region of non-overlapping muffin-tin (MT) spheres centered at nuclei and an interstitial region. The electronic states in the interstitial region are expanded in plane waves, whereas in the MT region the states are expanded in terms of spherical harmonics. All calculations were carried out for the lattice constants and the atomic coordinates determined from the Rietveld analysis of the X-ray diffraction spectrum of $Na_2Fe_2Se_2O$ [16]. The exchange–correlation potential was calculated using the generalized gradient approximation (GGA) technique within the density functional theory (DFT), employing the scheme developed by Perdew et al. [19]. A separation energy of −8.0 Ry between the valence and core states of individual atoms in the unit cell was chosen.

The radii of the MT spheres used in the calculations were 2.00 a.u. for Na, 1.80 a.u. for Fe, 2.10 a.u. for Se, and 1.90 a.u. for O. The plane-wave cut-off parameter $R_{MT} \times K_{MAX}$ (R_{MT} is the radius of the smallest sphere in the unit cell and K_{MAX} is the maximum K vector in the Fourier expansion of the plane waves in the interstitial region) value of 6.5 was used. The wave functions in the core regions were expanded to a maximum of $l = 12$ harmonics whereas the valence wave functions were expanded in spherical harmonics up to $l = 4$. A total number of 726 k-points was generated on a $21 \times 21 \times 21$ k-mesh in the irreducible wedge of the first Brillouin zone. An energy convergence criterion of 0.0001 Ry for successive iterations in the self-consistent field (SCF) cycles was chosen. Calculations of the antiferromagnetic state were carried out using a supercell of dimensions $2a \times 2a \times c$.

The ^{57}Fe Mössbauer measurements were conducted using standard Mössbauer spectrometers [20] operating in sine mode and a ^{57}Co(Rh) source, which was kept at room temperature for zero-field measurements and at the same temperature as that of the absorber for an in-field measurement. The spectrometers used for zero-field and in-field measurements were calibrated, respectively, with a 6.35-μm-thick α-Fe foil [21] and a Michelson interferometer [22], and the spectra were folded. The Mössbauer absorber was made in a glove box. The powder material was mixed with boron nitride and was put into a high-purity, 8-μm-thick Al disk container to ensure a uniform temperature over the whole absorber. The Mössbauer absorber was exposed to air for about 100 s when it was transported from the glove box to the Mössbauer cryostat in which it was kept in a static exchange gas atmosphere at the pressure of $\sim 7 \times 10^{-3}$ mbar. The surface density of the prepared Mössbauer absorber of 26.5 mg/cm^2 corresponds to an effective thickness parameter [20] $t_a = 5.2 f_a$, where f_a is the Debye–Waller factor of the absorber. Since $t_a > 1$, the resonance line shape of the Mössbauer spectrum was described using a transmission integral formula [23]. The source linewidth $\Gamma_s = 0.13$ mm/s and the background-corrected Debye–Waller factor of the source $f_s^* = 0.50$ were used in the fits of the Mössbauer spectra [23]. As the magnitude of the electric quadrupole interaction is comparable to that of the magnetic dipole interaction in the studied compound at temperatures below T_N, the ^{57}Fe Zeeman spectra were analyzed by means of a least-squares fitting procedure which entailed calculations of the positions and relative intensities of the absorption lines by numerical diagonalization of the full hyperfine interaction Hamiltonian [20].

3. Results and discussion

3.1. Ab-initio calculations

3.1.1. Nonmagnetic and magnetic states

The electronic band structure of the nonmagnetic, ferromagnetic, and antiferromagnetic states has been determined and is discussed below.

The nonmagnetic state of the $Na_2Fe_2Se_2O$ compound describes the high-temperature phase of this system. The electronic band structure of this nonmagnetic state is shown in Fig. 1(c). The absence of an energy gap across the Fermi level points to the metallic-like character of the studied system at high temperatures. In the vicinity of the Fermi level, one observes [Fig. 1(c)] a number of energy bands in different directions in the Brillouin zone. This leads to a high electrical conductivity in this state. Our calculations show that, as expected, the magnetic moments of all atoms in this nonmagnetic state are zero.

The spin-up and spin-down energy bands in the ferromagnetic state of $Na_2Fe_2Se_2O$ are shown in Fig. 1(a) and (b). One can notice the formation of a spin-dependent energy band gap. The maximum of the valence band lies about 0.1 eV below the Fermi level, whereas the minimum of the conduction band is located at about 1.3 eV above the Fermi level. This allows indirect interband transitions of energies larger than about 1.4 eV along the N–Γ direction. As can be seen from Fig. 1(a) and (b), the strong ferromagnetic coupling of the Fe magnetic moments is responsible for the localization of the Fe 3d states in the spin-up configuration. This prevents the existence of the electronic states above the Fermi level and creates a band gap. On the contrary, for the spin-down configuration one can clearly observe the metallic behavior [Fig. 1(b)]. This clear spin-dependent distinction in the electronic properties of the Fe 3d states can be potentially useful in spintronics applications where one can open a channel for the spin-down currents which see no potential barrier, whereas the spin-up currents are blocked. This leads to a spin-polarized current that can be of important use in quantum computation (for instance, the spin-polarized current can lead to distinct bits of information, very much similar to the traditional "0" and "1" used in ordinary computation systems).

The values of the calculated magnetic moments for the ferromagnetic state of $Na_2Fe_2Se_2O$ [Fig. 2(a)] are listed in Table 1. A strong magnetic coupling of the large Fe magnetic moment (3.23 μ_B) may lead to the induced magnetic moments on the Se and O atoms.

Three different in-plane antiferromagnetic spin configurations, that are often realized in layered parent compounds of Fe-based superconductors [2,4,24], were considered in the previous *ab-initio* study of $Na_2Fe_2Se_2O$ [17]. The antiferromagnetically coupled Fe magnetic moments were assumed to lie in the a-b plane along the [1 1 0] direction, hence creating a 2D magnetic system. A similar antiferromagnetic order was reported [15] to exist in the $Na_2Ti_2Pn_2O$ (Pn = Sb, As) pnictide oxides. The three antiferromagnetic spin configurations that could occur in $Na_2Fe_2Se_2O$ are shown in Fig. 2(b)–(d). In the stripe-like antiferromagnetic configuration [Fig. 2(b)], the chains of Fe magnetic moments are coupled ferromagnetically with an antiferromagnetic coupling between the adjacent chains. The checkerboard antiferromagnetic configuration [Fig. 2(c)] has an Fe magnetic moment coupled antiferromagnetically with its nearest-neighbor Fe magnetic moments. In the blocked checkerboard antiferromagnetic configuration [Fig. 2(d)], four adjacent Fe atoms form a $\sqrt{2}a \times \sqrt{2}a$ block in which all Fe magnetic moments are coupled ferromagnetically, whereas the block is antiferromagnetically coupled to the adjacent blocks in a checkerboard fashion. Energy considerations show [17] that the lowest total energy is for the blocked checkerboard antiferromagnetic configuration, and therefore this configuration appears to be the most probable.

An inspection of the band structure of the blocked checkerboard antiferromagnetic configuration [Fig. 1(d)] shows that the bands which are not in the vicinity of the Fermi level are unaltered and remain at the same energy as the bands corresponding to the nonmagnetic state [Fig. 1(c)]. The band structure in the vicinity of the Fermi level shows a small energy gap [Fig. 1(d)] that implies the existence of a Mott insulating state [25].

Our calculations yield the value of 3.186 μ_B for the Fe magnetic moment (Table 1) in the blocked checkerboard antiferromagnetic configuration. There are no induced magnetic moments on the Na, Se, and O atoms. The total energy for the blocked checkerboard antiferromagnetic configuration is lower than that for the ferromagnetic configuration (Table 1), thus confirming that the former is the preferred spin configuration in the studied compound.

3.1.2. Hyperfine-interaction parameters

Experiments carried out with Mössbauer spectroscopy technique reveal the three most prominent hyperfine-interaction parameters: the isomer shift, δ_0, the hyperfine magnetic field, H, and the principal component of the electric field gradient (EFG) tensor, V_{zz}, with the asymmetry parameter, η [20]. Knowing the crystal structure of a studied compound, these parameters can be also obtained from the first-principles calculations [26].

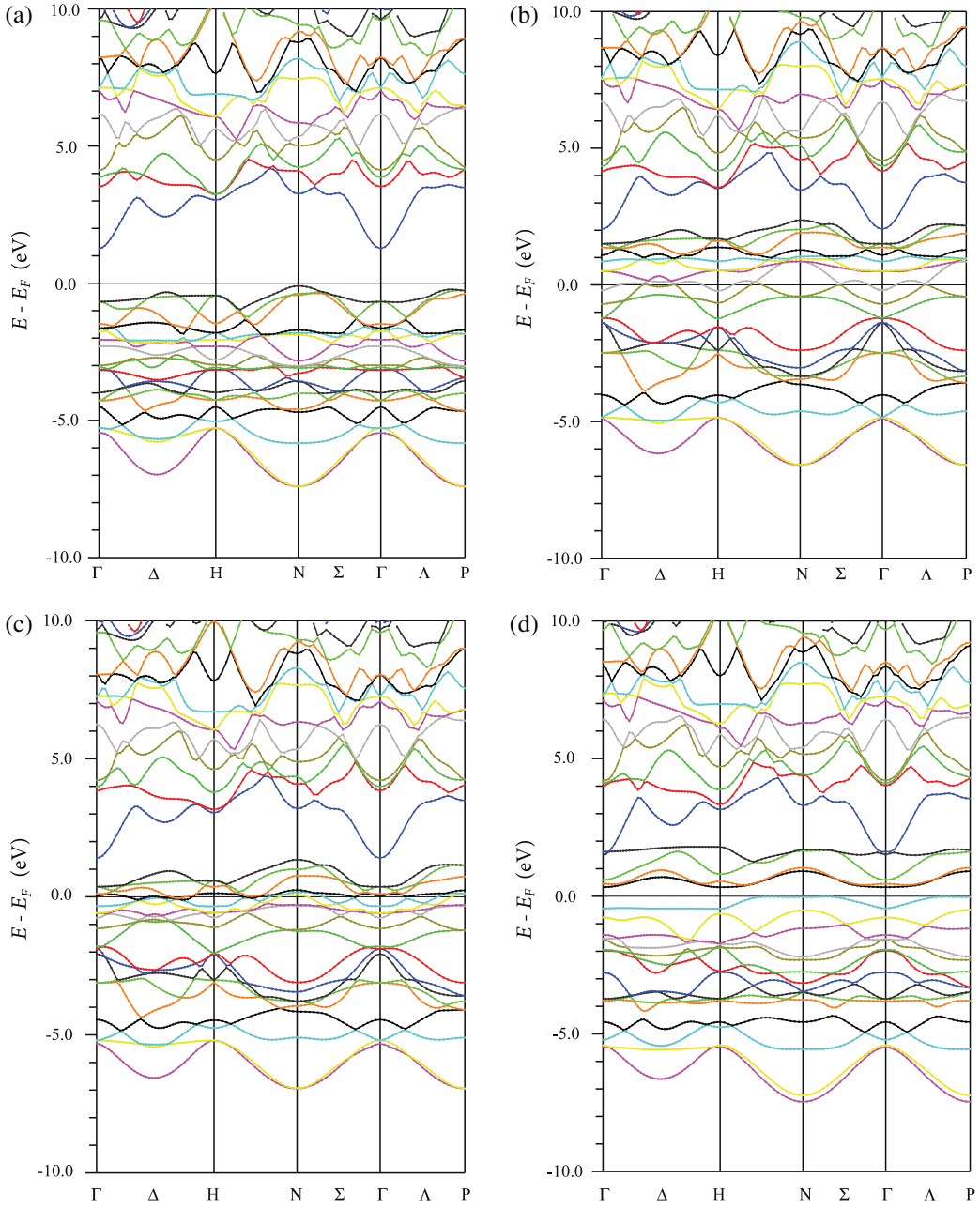

Fig. 1. Energy band structure of $Na_2Fe_2Se_2O$ in various states: spin up (a) and spin down (b) ferromagnetic state, nonmagnetic state (c), and blocked checkerboard antiferromagnetic state (d).

The isomer shift is proportional to the total electron density at the Mössbauer nucleus $\rho(0)$

$$\delta_0 = \alpha(\rho(0) - \rho_{ref}(0)), \tag{1}$$

where $\rho_{ref}(0)$ is the electron density in a reference compound and α is a calibration constant. In calculating $\rho(0)$, relativistic spin–orbit effects were invoked in order to account for the possibility of the penetration of the $p_{1/2}$ electrons into the ^{57}Fe nuclei. As a reference compound, an α-Fe (with the *bcc* structure and the lattice constant of 2.8665 Å) was chosen. The calculated values of $\rho(0)$ and $\rho_{ref}(0)$ are, respectively, 15306.521 and 15309.918 a.u.$^{-3}$. Using the calibration constant $\alpha = -0.291$ a.u.^{3} (mm/s) (Ref. [27]), Eq. (1) yields $\delta_0 = 0.988$ mm/s.

The hyperfine magnetic field in a magnetic material consists of three distinct contributions: the Fermi contact term H_c, the magnetic dipolar term, H_{dip}, and the orbital moment term, H_{orb} [20]. Of these, the first term is usually significantly larger in magnitude than the last two terms. The Fermi contact term is given by

$$H_c = \frac{8\pi}{3}\mu_B^2(\rho_\uparrow(0) - \rho_\downarrow(0)), \tag{2}$$

where $\rho_\uparrow(0)$ and $\rho_\downarrow(0)$ are the spin-up and spin-down densities at the Mössbauer nucleus, respectively. The magnitude of H_c in $Na_2Fe_2Se_2O$ calculated from Eq. (2) is 215 kOe.

The calculations of V_{zz} and η yielded the values of 11.113×10^{21} V/m^2 and 0.0, respectively. The dominant contribution to V_{zz} ($\sim 8 \times 10^{21}$ V/m^2) comes from the electrons with a strong *d* character, and the remaining contribution ($\sim 3 \times 10^{21}$ V/m^2) is the result of the *s*–*d* orbital hybridization. V_{zz} is dominated by the contribution from a region very close to the

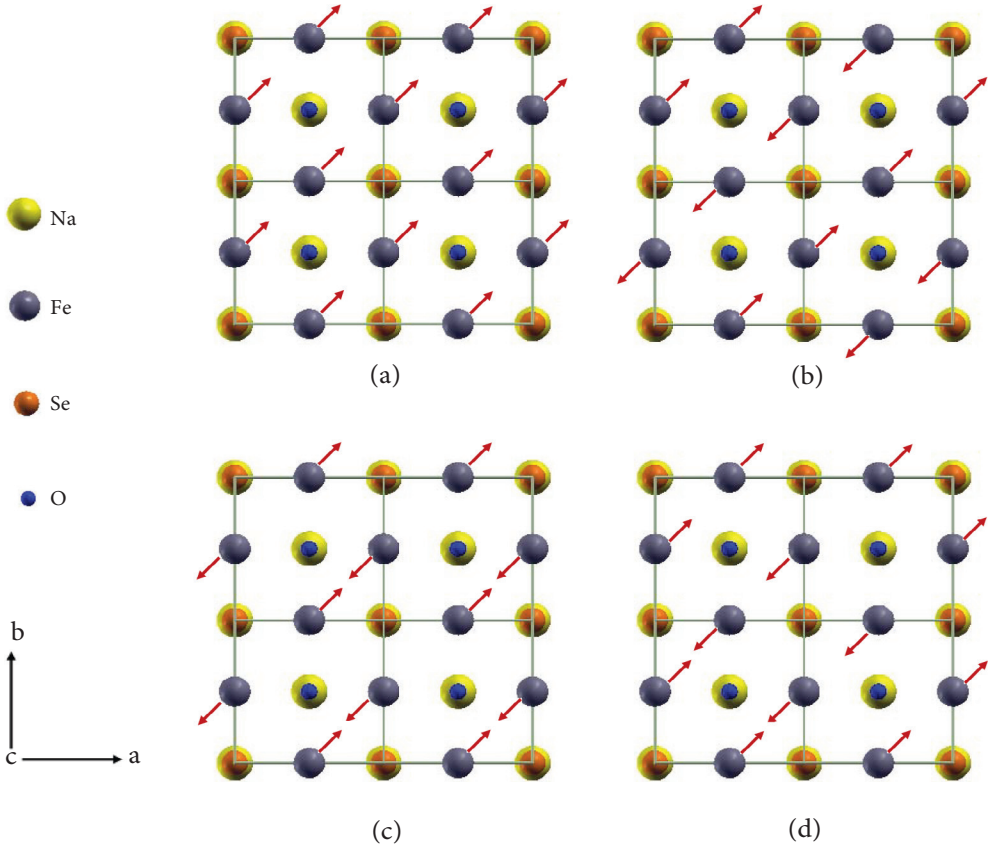

Fig. 2. In-plane arrangement of Fe magnetic moments for $Na_2Fe_2Se_2O$ in the ferromagnetic state (a), stripe-like antiferromagnetic state (b), checkerboard antiferromagnetic state (c), and blocked checkerboard antiferromagnetic state (d).

Table 1
The magnetic moments μ of Na, Fe, Se, and O atoms in ferromagnetic and blocked checkerboard antiferromagnetic states of $Na_2Fe_2Se_2O$ and the total-energy difference ΔE (with respect to the nonmagnetic state).

State	μ_{Na} (μ_B)	μ_{Fe} (μ_B)	μ_{Se} (μ_B)	μ_O (μ_B)	ΔE (eV)
Ferromagnetic	0	3.23	0.18	0.29	−0.2584
Antiferromagnetic	0	3.19	0	0	−0.2739

Mössbauer nucleus: the contribution from the region within 20% of the MT radius (10.784×10^{21} V/m^2) almost reaches the saturation value of V_{zz}.

3.2. Mössbauer spectroscopy

The room-temperature ^{57}Fe Mössbauer spectrum of $Na_2Fe_2Se_2O$ (Fig. 3) consists of two asymmetric quadrupole doublets and a Zeeman sextet. The asymmetry of the two quadrupole doublets is caused by preferred orientation (texture) in the polycrystalline Mössbauer absorber (the tendency of the polycrystalline grains of a layer-structure compound to align themselves predominantly with the *c*-axis perpendicular to the plane of the absorber). This is confirmed by the observation that this asymmetry almost disappears (the right inset in Fig. 3) if the spectrum is measured at the so-called "magic angle"; in such a measurement the normal to the Mössbauer absorber plane and the direction of the γ-rays form an angle of 54.7° [28]. The major quadrupole doublet originates from the compound studied. The minor quadrupole doublet is due to the impurity in the absorber that was produced during its short exposure to air. This is corroborated by the fact that the spectral weight of this minor quadrupole doublet significantly increased in the magic-angle spectrum (the right inset in Fig. 3) that was measured for 15 h with the Mössbauer absorber accidentally exposed to air at the pressure of ~1.5 mbar. The Zeeman sextet component originates from a trace amount of Fe metal impurity.

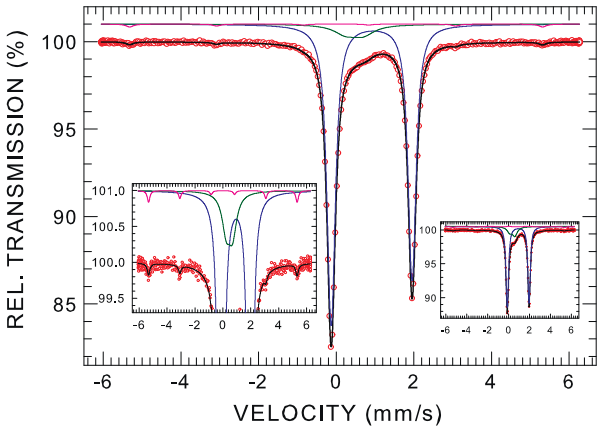

Fig. 3. ^{57}Fe Mössbauer spectrum of $Na_2Fe_2Se_2O$ at 296.8 K fitted (black solid line) with an asymmetric quadrupole doublet (blue solid line) due to main phase, an asymmetric quadrupole doublet (dark green solid line) due to air-environment induced impurity, and a Zeeman pattern (pink solid line) originating from Fe impurity. The left inset shows the spectrum with an enlarged vertical scale and the right inset shows the spectrum measured at the magic angle, as described in the text. The zero-velocity origin is relative to α-Fe at room temperature. (For interpretation of the references to colour in this figure legend, the reader is referred to the web version of this article.)

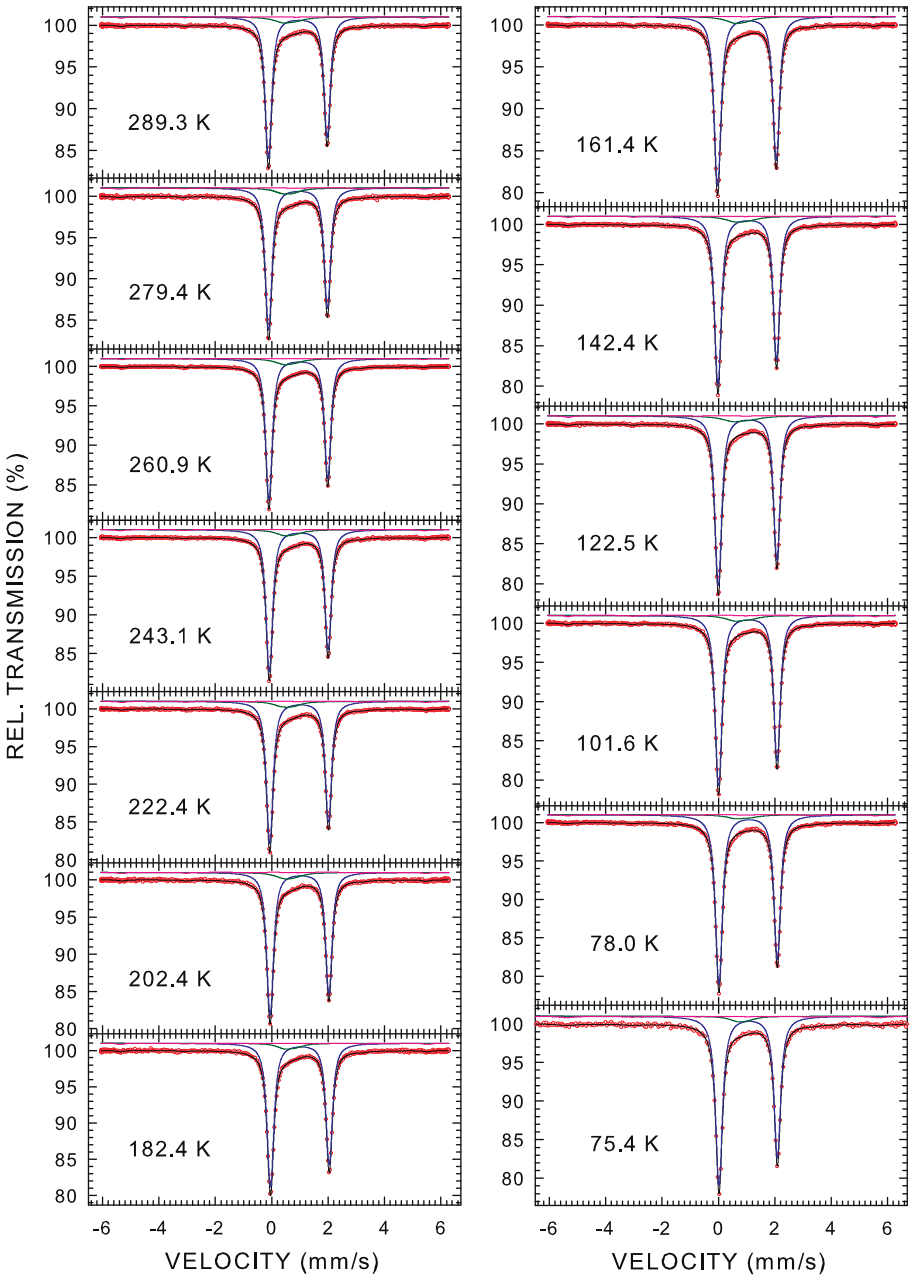

Fig. 4. ^{57}Fe Mössbauer spectra of $Na_2Fe_2Se_2O$ at the indicated temperatures fitted (black solid lines) with an asymmetric quadrupole doublet (blue solid lines) due to main phase, an asymmetric quadrupole doublet (dark green solid lines) due to air-environment induced impurity, and a Zeeman pattern (pink solid line) originating from Fe impurity. The zero-velocity origin is relative to α-Fe at room temperature. (For interpretation of the references to colour in this figure legend, the reader is referred to the web version of this article.)

The fit of the room-temperature spectrum (Fig. 3) with these three components yields the following parameters: the absorber linewidth Γ_a, the center shift δ (relative to α-Fe at 298 K), the effective quadrupole splitting $\tilde{\Delta} = \frac{1}{2}eQ|V_{zz}|\sqrt{1+\eta^2/3}$ (where e is the proton charge and Q is the electric quadrupole moment of the ^{57}Fe nucleus [29]), the hyperfine magnetic field H, and the spectral area A [20]. The values of these parameters corresponding to these three components are $\Gamma_{a1} = 0.132(2)$ mm/s, $\delta_1 = 0.919(1)$ mm/s, $\tilde{\Delta}_1 = 2.083(1)$ mm/s, $A_1 = 91.6(1)\%$, $\Gamma_{a2} = 0.579(49)$ mm/s, $\delta_2 = 0.465(29)$ mm/s, $\tilde{\Delta}_2 = 0.449(28)$ mm/s, $A_2 = 7.0(4)\%$, and $\Gamma_{a3} = 0.089(6)$ mm/s, $\delta_3 = 0.002(3)$ mm/s, $H_3 = 329.6(8)$ kOe, $A_3 = 1.3(2)\%$.

The values of δ_1 and Δ_1 are typical of high-spin Fe^{2+}ions [20]. The ferrous state of Fe atoms can be expected from the ionic formula $Na_2^{1+}Fe_2^{2+}Se_2^{2-}O_{2-}$ in which the usual oxidation numbers are assigned to Na, Se, and O atoms. ^{57}Fe Mössbauer spectra similar to the room-temperature spectrum (Fig. 3) were recorded at other temperatures down to 75.4 K (Fig. 4). The presence of the major asymmetric quadrupole doublet down to 75.4 K indicates that the magnetic ordering temperature of $Na_2Fe_2Se_2O$ must be below 75.4 K. The temperature dependence of hyperfine parameters derived from the fits of the spectra in Figs. 3 and 4 will be discussed later.

The ^{57}Fe Mössbauer spectra of $Na_2Fe_2Se_2O$ at 5.8 K, i.e., at the temperature much below the magnetic ordering temperature, measured in the external magnetic fields $H_{ext} = 0$ and 90 kOe applied parallel to the γ-ray propagation direction are shown in Fig. 5. The zero-field spectrum can be fitted well with one

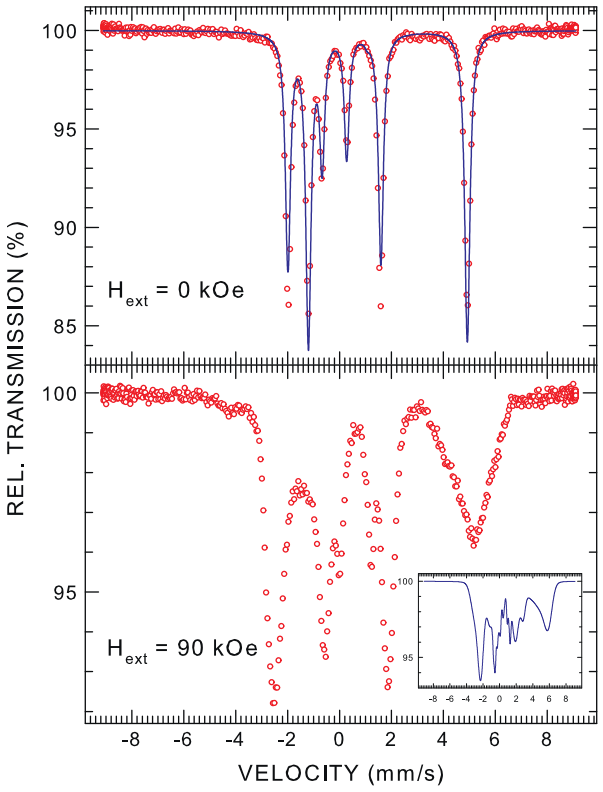

Fig. 5. ^{57}Fe Mössbauer spectra of $Na_2Fe_2Se_2O$ at 5.8 K in zero and 90 kOe external magnetic field H_{ext} applied parallel to the direction of the γ-rays. The $H_{ext} = 0$ kOe spectrum is fitted (blue solid line) to a Zeeman pattern, as described in the text. The inset shows a $H_{ext} = 90.0$ kOe simulated spectrum, as described in the text. The zero-velocity origin is relative to the source. (For interpretation of the references to colour in this figure legend, the reader is referred to the web version of this article.)

Zeeman pattern originating from the compound studied (a Zeeman pattern due to an Fe impurity is not included in the fit due to its negligible spectral weight; a possible Zeeman pattern with a small spectral weight due to the impurity caused by the sample's short exposure to the air is also not included in the fit as it overlaps with, and is completely overhelmed by, the Zeeman pattern due to the main phase). The Fe atoms are located at the 4*c* sites with the point symmetry *mmm*. (Ref. [16]); this allows $\eta > 0$. The values of the parameters obtained from the fit are $\Gamma_a = 0.045(3)$ mm/s, $H = 190.4(2)$ kOe, the quadrupole splitting $\Delta = 2.039(3)$ mm/s ($\Delta = \frac{1}{2} eQV_{zz}$), $\eta = 0.0(1)$, and the angle between V_{zz} and $H, \alpha = 5.0(7)^\circ$. The value $\Delta = 2.039(3)$ mm/s implies [29] that $V_{zz} = 13.070(19) \times 10^{21}$ V/m^2. Whereas the experimental value of η agrees very well the calculated one, the experimental value of V_{zz} is 17.6% larger than the calculated value of 11.113×10^{21} V/m^2. This, however, does not mean that the calculated V_{zz} is imprecise as the precision of the experimentally determined V_{zz} is dictated by the accuracy of the *Q* value which is 13.3% [29].

The ^{57}Fe Mössbauer spectra of a magnetically ordered compound measured in zero external magnetic field give information on the magnitude and direction of the hyperfine magnetic field, and thus of the Fe magnetic moment, but not on the type of magnetic ordering of these moments. The type of magnetic ordering can be inferred from Mössbauer spectra measured in a strong enough external magnetic field [30]. The most striking feature of the $H_{ext} = 90$ kOe spectrum (Fig. 5) is its dramatic broadening as compared to the $H_{ext} = 0$ kOe spectrum. As is explained below, this broadened spectrum constitutes experimental proof of the antiferromagnetic ordering of the Fe magnetic moments in the compound studied.

There are two types of behavior of a polycrystalline uniaxial antiferromagnet in H_{ext} [31]. When the magneto-crystalline anisotropy energy is small, the antiferromagnetic spin-system will flop, i.e., the spin-system will rotate perpendicular to H_{ext}. In this case, H_{ext} will add in quadrature to H and all ^{57}Fe nuclei will experience the same effective field $H_{eff} = \sqrt{H_{ext}^2 + H^2}$, and consequently no broadening will be produced. Clearly, this is not the case here. In the second case, for a high magneto-crystalline anisotropy energy, the effective field $H_{eff} = \sqrt{H_{ext}^2 + H^2 + 2H_{ext}H\cos\theta}$ (θ is the angle between H_{ext} and H_{eff}) will range from $|H - H_{ext}|$ to $|H + H_{ext}|$, with the probability of the occurrence of a particular H_{eff} value $p(H_{eff}) = H_{eff}/(2HH_{ext})$ [32]. This distribution of the effective fields will lead qualitatively to the broadening observed here (Fig. 5). To be more quantitative, we have simulated an expected $H_{ext} = 90$ kOe spectrum (the quadrupole interaction could not be rigorously included in the simulation for the reasons elaborated in Ref. [32]) as a superposition of the six $p(H_{eff})$-weighted Zeeman patterns with H_{eff} values of 100.4, 136.4, 172.4, 208.4, 244.4, and 280.4 kOe (inset in Fig. 5). The simulated spectrum reflects the shape of the experimental spectrum reasonably well, thus validating the claim of antiferromagnetic coupling of the Fe magnetic moments in the compound studied.

The ^{57}Fe Mössbauer spectrum of $Na_2Fe_2Se_2O$ measured at temperatures below the Néel temperature T_N are shown in Fig. 5. They can be fitted well with a Zeeman pattern originating from the main phase. The spectra measured at 72.2, 73.2 and 74.4 K, i.e., at temperatures in the vicinity of T_N, show that magnetically ordered (a Zeeman pattern) and paramagnetic (an asymmetric quadrupole doublet pattern) material coexist, with the spectral weight of the doublet pattern increasing at the expense of the spectral weight of the Zeeman pattern as the temperature approaches T_N. Such a coexistence may be attributable to a small spreading out of T_N resulting from some inhomogeneity of the sample's composition.

Fig. 7(a) shows the temperature dependence of the absorption spectral area A of $Na_2Fe_2Se_2O$ derived from the fits of the Mössbauer spectra in Figs. 3, 4 and 6. This area is proportional to the absorber Debye–Waller factor f_a, which is given in the Debye theory by [20]

$$f_a(T) = \exp\left\{-\frac{3}{4}\frac{E_\gamma^2}{Mc^2 k_B \Theta_D}\left[1 + 4\left(\frac{T}{\Theta_D}\right)^2 \int_0^{\Theta_D/T} \frac{x\,dx}{e^x - 1}\right]\right\}, \quad (3)$$

where M is the mass of the Mössbauer nucleus, c is the speed of light, k_B is the Boltzmann constant, E_γ is the energy of the Mössbauer transition, and Θ_D is the Debye temperature. The fit of the experimental dependence $A(T)$ [Fig. 7(a)] to Eq. (3) yields $\Theta_D = 260(4)$ K.

The temperature dependence of $\delta(T)$, determined from the fits of the Mössbauer spectra in Figs. 3, 4 and 6, is shown in Fig. 7(b). $\delta(T)$ is given by

$$\delta(T) = \delta_0 + \delta_{SOD}(T), \quad (4)$$

where δ_0 is the intrinsic isomer shift and $\delta_{SOD}(T)$ is the second-order Doppler (SOD) shift which depends on the lattice vibrations of the Fe atoms [20]. In terms of the Debye approximation of the lattice vibrations, $\delta_{SOD}(T)$ is expressed [20] in terms of Θ_D as

$$\delta_{SOD}(T) = -\frac{9}{2}\frac{k_B T}{Mc}\left(\frac{T}{\Theta_D}\right)^3 \int_0^{\Theta_D/T} \frac{x^3\,dx}{e^x - 1}. \quad (5)$$

By fitting the experimental data $\delta(T)$ [Fig. 7(b)] to Eq. (4), the quantities δ_0 and Θ_D were found to be 1.065(3) mm/s and 295(5) K, respectively. We note here that the calculated

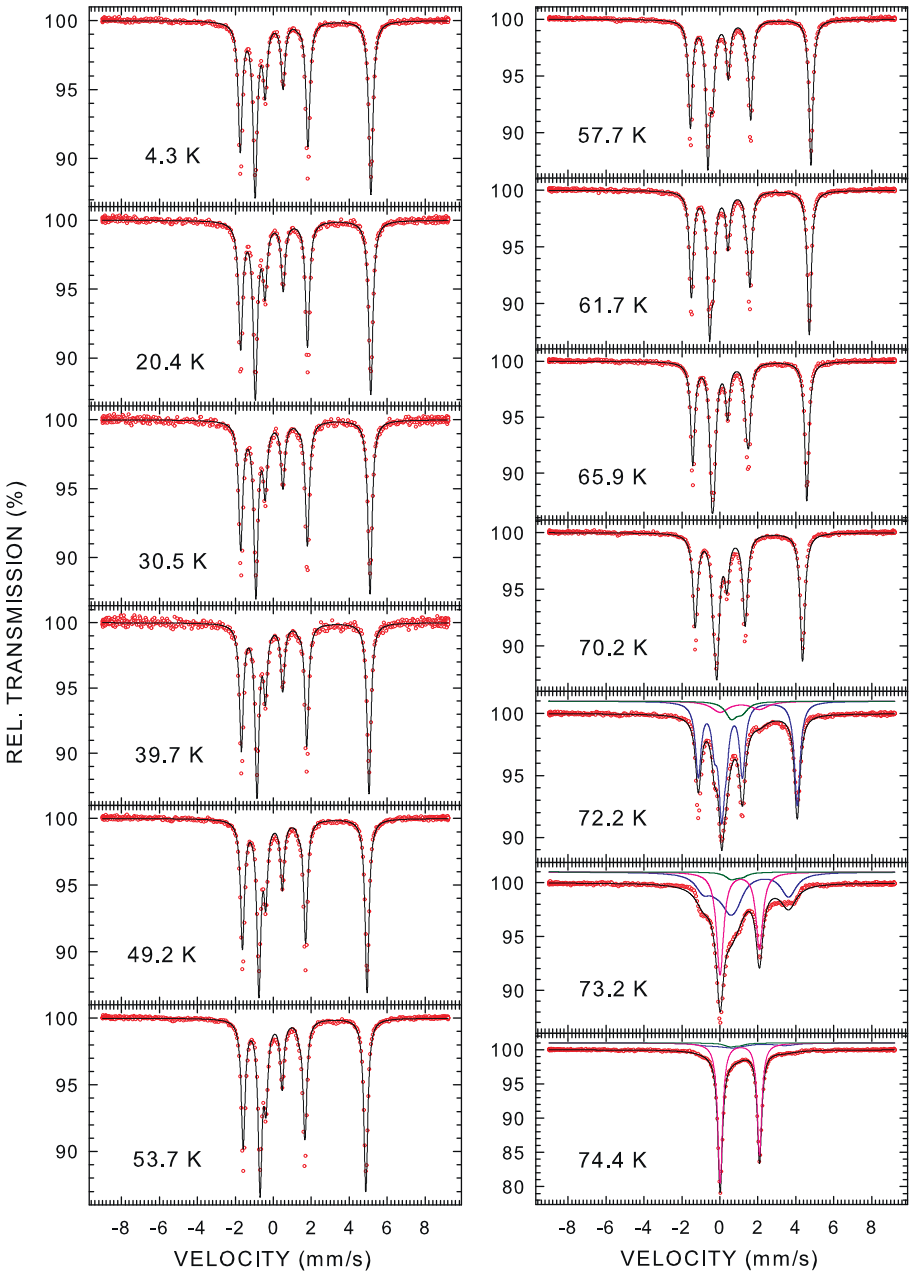

Fig. 6. ^{57}Fe Mössbauer spectra of $Na_2Fe_2Se_2O$ at the indicated temperatures fitted (black solid lines) with a Zeeman pattern. The spectra at 72.2, 73.2, and 74.4 K are fitted with three components – a Zeeman pattern (blue solid lines) due to the main phase, an asymmetric quadrupole doublet (pink solid lines) due to the main phase, and an asymmetric quadrupole doublet (dark green solid lines) due to air-environment induced impurity, as described in the text. The zero-velocity origin is relative to α-Fe at room temperature. (For interpretation of the references to colour in this figure legend, the reader is referred to the web version of this article.)

$\delta_0 = 0.998$ mm/s is very close the experimental value of 1.065(3) mm/s, which gives credence to the reliability of the *ab-initio* calculations of the hyperfine-interaction parameters.

The value of Θ_D determined from the $A(T)$ data is clearly smaller than the one derived from the $\delta(T)$ data. In fact, the Θ_D values determined from the $A(T)$ data are always smaller than the ones obtained from the $\delta(T)$ data. This results from the way in which Θ_D is calculated. Let's recall that f_a and δ_{SOD} are related to the mean-square vibrational displacement $\langle x^2\rangle$ and the mean-square velocity $\langle v^2\rangle$ of the Mössbauer nucleus, respectively [20]. Because $\langle x^2\rangle$ weights the phonon frequency distribution by ω^{-1} whilst $\langle v^2\rangle$ weights it by ω^{+1} [33], the Θ_D values derived from the $A(T)$ data are necessarily lower than those determined from the $\delta(T)$ data. The weighted average of these two Θ_D values is 274(3) K. It is in an excellent agreement with the value of 277 K determined from specific heat measurements. [16].

Fig. 7(c) shows the temperature dependence of the quadrupole splitting Δ derived from the fits of the Mössbauer spectra in Figs. 3–6. One observes that Δ is approximately constant at high temperatures above ~150 K and then clearly decreases at lower temperatures. We suggest that this decrease is probably caused by a possible subtle structural transition below ~150 K, as observed in a structurally similar compound $La_2Fe_2Se_2O_3$ [34].

The temperature dependences of H and α determined from the fits of the Mössbauer spectra in Figs. 5 and 6 are displayed in Fig. 8. The $H(T)$ dependence in Fig. 8(a) was fitted in terms of the Bean–Rodbell exchange model [35] in which the reduced magnetization $\sigma = M(T)/M(0)$, and hence (assuming proportionality between M

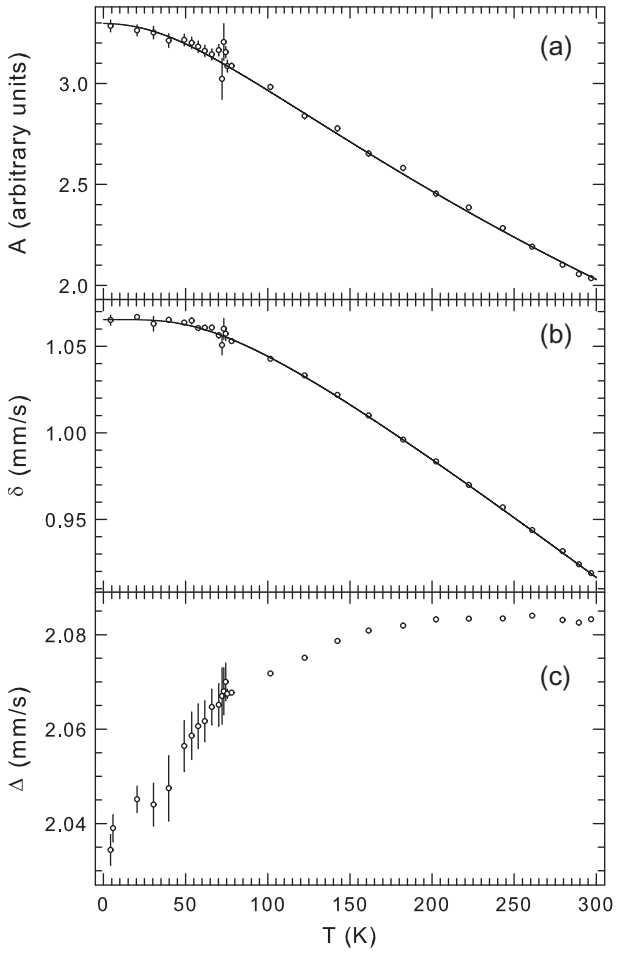

Fig. 7. Temperature dependence of (a) the absorption spectral area A, (b) the center shift δ, and (c) the quadrupole splitting Δ. The solid lines are the fits to Eq. (3) in (a) and to Eq. (4) in (b), as explained in the text.

and H) the reduced hyperfine magnetic field $\sigma = H(T)/H(0)$, is given by

$$\sigma = B_S\left[\frac{3S}{S+1}\frac{\sigma}{\Theta}\left(1+\frac{3}{80}\frac{(2S+1)^4-1}{S(S+1)^3}\zeta\sigma^2\right)\right], \quad (6)$$

where B_S is the Brillouin function for spin S, $\Theta = T/T_N$, and ζ is the order parameter of the transition. For an ideal second-order transition $\zeta = 0$ and for the first-order transition $\zeta > 1$. The ζ values between 0 and 1 correspond to intermediate-order transitions [35]. As the δ and Δ values indicate that Fe^{2+} ions in the compound studied are in a high-spin configuration, we used $S = 2$ in fitting the $H(T)$ data to Eq. (6). The fit [Fig. 8(a)] yielded $H(0) = 189.6(1.8)$ kOe, $T_N = 74.7(5)$ K, and $\zeta = 1.22(19)$. We note that the experimental value of $H(0)$ is quite close the calculated H_c contribution of 215 kOe. This seems to confirm the general observation that the $|H_{dip} + H_{orb}|$ contribution (about 25 kOe in our case) is about an order of magnitude smaller than the H_c contribution. The value of ζ indicates that the nature of the antiferromagnetic transition is first order. Since H is, to a first approximation, proportional to the on-site magnetic moment of iron atoms μ_{Fe} through the relation $H = a\mu_{Fe}$, where the value of the proportionality constant a is compound specific [36], one can estimate μ_{Fe} from the measured H. In converting $H(0)$ to $\mu_{Fe}(0)$, we used $a = 62.6(1.9)$ kOe/μ_B, which results from $H(4.2\text{ K}) = 206(5)$ kOe and $\mu_{Fe}(16\text{ K}) = 3.1(1)$ μ_B determined from a Mössbauer and a neutron diffraction study of a

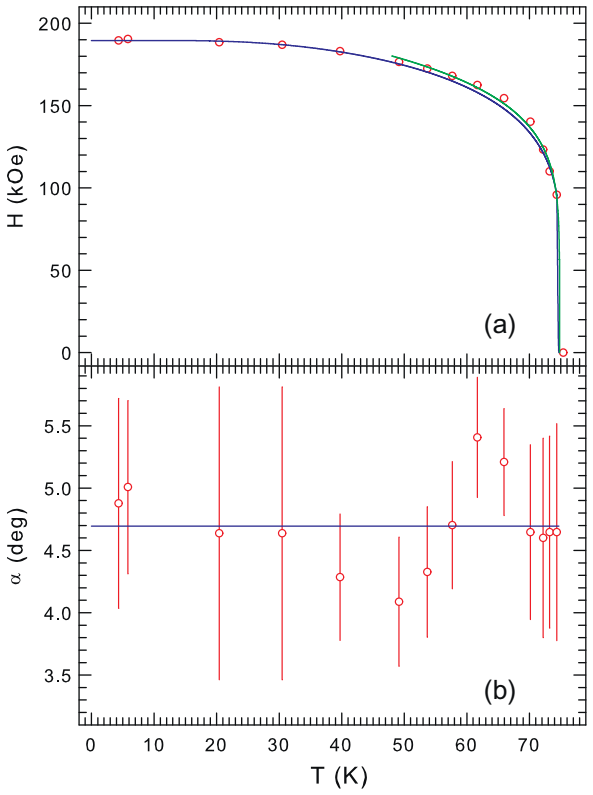

Fig. 8. Temperature dependence of (a) the hyperfine magnetic field H and (b) the angle α between V_{zz} and H. The blue and green solid lines in (a) are the fits to Eq. (6) and to the power-law, respectively.

structurally similar compound $Sr_2Fe_2S_2F_2O$ [37,38]. Thus, the value of $\mu_{Fe}(0)$ in $Na_2Fe_2Se_2O$ is 3.0(1) μ_B. The value of $\mu_{Fe}(0)$ is in rather good agreement with the calculated value of 3.19 μ_B (Table 1).

We also fitted the $H(T)$ data for temperatures above $0.66T_N$ to the power-law function, $H(T) \propto (1 - T/T_N)^{\beta}$. Such a fit [Fig. 8(a)] yielded $T_N = 74.8(2)$ K and $\beta = 0.159(12)$. The β value is close to the theoretical value of 0.125 expected for a 2D square planar Ising system [39]. The angle α does not change with temperature [Fig. 8(b)] and its average value is 4.7(1)°.

4. Conclusions

The results of Mössbauer spectroscopy measurements and of *ab-initio* calculations of the electronic energy bands and hyperfine-interaction properties of the recently discovered $Na_2Fe_2Se_2O$ compound are presented. We confirm that $Na_2Fe_2Se_2O$ is a Mott insulator. We show experimentally that in the ground state the studied compound is an antiferromagnet with the Néel temperature $T_N = 74.8(2)$ K and with the Fe magnetic moment of 3.0(1) μ_B. Good agreement is observed between the calculated hyperfine-interaction and magnetic parameters and the corresponding measured ones. We find that the Debye temperature of $Na_2Fe_2Se_2O$ is 274(3) K.

Acknowledgments

This work was supported by the Natural Sciences and Engineering Research Council of Canada. We thank Pu Wang for technical help with WIEN2k, and Junbao He and Gen-Fu Chen for providing the sample of $Na_2Fe_2Se_2O$.

References

[1] H.-H. Wen, S. Li, Annu. Rev. Condens. Matter Phys. 2 (2011) 121. and references therein.
[2] G.R. Stewart, Rev. Mod. Phys. 83 (2011) 1589. and references therein.
[3] J. Wen, G. Xu, G. Gu, J.M. Tranquada, R.J. Birgenau, Rep. Prog. Phys. 74 (2011) 124503. and references therein.
[4] D. Johrendt, J. Mater. Chem. 21 (2011) 13726. and references therein.
[5] D. Johrendt, H. Hosono, R.-D. Hoffmann, R. Pöttgen, Z. Kristallogr. 226 (2011) 435. and references therein.
[6] A. Adam, H.-U. Schuster, Z. Anorg. Allg. Chem. 584 (1990) 150.
[7] J.G. Bednorz, K.A. Müller, Z. Phys. B 64 (1986) 189.
[8] T.C. Ozawa, E.A. Axtell III, T.C. Ozawa, S.M. Kauzlarich, R.R.P. Singh, J. Solid State Chem. 134 (1997) 423.
[9] T.C. Ozawa, R. Pantoja, E.A. Axtell III, S.M. Kauzlarich, J.F. Greedan, M. Bieringer, J.W. Richardson Jr., J. Solid State Chem. 153 (2000) 275.
[10] T.C. Ozawa, S.M. Kauzlarich, M. Bieringer, J.F. Greedan, Chem. Mater. 13 (2001) 1804.
[11] T.C. Ozawa, S.M. Kauzlarich, J. Cryst. Growth 265 (2004) 571.
[12] R.H. Liu, D. Tan, Y.A. Song, Q.J. Li, Y.J. Yan, J.J. Ying, Y.L. Xie, X.F. Wang, X.H. Chen, Phys. Rev. B 80 (2009) 144516.
[13] W.E. Pickett, Phys. Rev. B 58 (1998) 4335.
[14] F.F. de Biani, P. Alemany, E. Canadell, Inorg. Chem. 37 (1998) 5807.
[15] X.-W. Yan, Z.-Y. Lu, J. Phys.: Condens. Matter 25 (2013) 365501.
[16] J.B. He, D.M. Wang, H.L. Shi, H.X. Yang, J.Q. Li, G.F. Chen, Phys. Rev. B 84 (2011) 205212.
[17] D.V. Suetin, I.R. Shein, A.L. Ivanovskii, Solid State Commun. 152 (2012) 1969.
[18] P. Blaha, K. Schwartz, G. Madsen, D. Kvasnicka, J. Luitz, WIEN2k, An Augmented Plane Wave Plus Local Orbitals Program for Calculating Crystal Properties, Karlheinz Schwarz, Technical Universität Wien, Austria, 1999.
[19] J.P. Perdew, S. Burke, M. Ernzerhof, Phys. Rev. Lett. 77 (1996) 3865.
[20] N.N. Greenwood, T.C. Gibb, Mössbauer Spectroscopy, Chapman and Hall, London, 1971; P. Gütlich, E. Bill, A. Trautwein, Mössbauer Spectroscopy and Transition Metal Chemistry, Springer, Berlin, 2011.
[21] Certificate of Calibration, Iron Foil Mössbauer Standard, Natl. Bur. Stand. (U.S.) Circ. No. 1541, in: J.P. Cali (Ed.), U.S. GPO, Washington, D.C., 1971.
[22] B.F. Otterloo, Z.M. Stadnik, A.E.M. Swolfs, Rev. Sci. Instrum. 54 (1983) 1575.
[23] S. Margulies, J.R. Ehrman, Nucl. Instrum. Methods 12 (1961) 131; G.K. Shenoy, J.M. Friedt, H. Maletta, S.L. Ruby, in: I.J. Gruverman, C.W. Seidel, D.K. Dieterly (Eds.), Mössbauer Effect Methodology, vol. 10, Plenum, New York, 1974, p. 277.
[24] M.D. Lumsden, A.D. Christianson, J. Phys.: Condens. Matter 22 (2010) 203203. and references therein..
[25] L. Craco, M.S. Laad, S. Leoni, J. Phys.: Condens. Matter 26 (2014) 145602.
[26] P. Blaha, J. Phys.: Conf. Series 217 (2010) 012009.
[27] U.D. Wdowik, K. Reubenbauer, Phys. Rev. B 76 (2007) 155118.
[28] T. Ericsson, R. Wäppling, J. Phys. (Paris), Colloq. 37 (1976) C6–719.
[29] G. Martínez-Pinedo, P. Schwerdtfeger, E. Caurier, K. Langanke, W. Nazarewich, T. Söhnel, Phys. Rev. Lett. 87 (2001) 062701.
[30] C.E. Johnson, J. Phys. D 29 (1996) 2266. and references therein.
[31] J. Chappert, J. Phys. (Paris), Colloq. 35 (1974) C6–71. and references therein.
[32] G.K. Wertheim, D.N.E. Buchanan, J.H. Wernick, Solid State Commun. 8 (1970) 2173.
[33] R.M. Housley, F. Hess, Phys. Rev. 146 (1966) 517.
[34] D.G. Free, S.O. Evans, Phys. Rev. B 81 (2010) 214433.
[35] C.P. Bean, D.S. Rodbell, Phys. Rev. 126 (1962) 104.
[36] Z.M. Stadnik, P. Wang, J. Żukrowski, T. Noji, Y. Koike, J. Phys.: Condens. Matter 25 (2013) 416008. and references therein.
[37] H. Kabbour, E. Janod, B. Corraze, M. Danot, C. Lee, M.-H. Whangbo, L. Cario, J. Am. Chem. Soc. 130 (2008) 8261.
[38] L.L. Zhao, S. Wu, J.K. Wang, J.P. Hodges, C. Broholm, E. Morosan, Phys. Rev. B 87 (2013) 020406(R).
[39] L. Onsager, Phys. Rev. 65 (1944) 117.